MODELING AND CONTROL OF AN ODYSSEY III AUV THROUGH SYSTEM IDENTIFICATION TESTS

Mark E. Rentschler
Research Assistant
Massachusetts Institute of Technology
Cambridge, MA 02139
mrentsch@mit.edu

Franz S. Hover
Principal Research Engineer
Massachusetts Institute of Technology
Cambridge, MA 02139
hover@mit.edu

Chryssostomos Chryssostomidis
Director, MIT Sea Grant College Program
Massachusetts Institute of Technology
Cambridge, MA 02139
chrys@mit.edu

Abstract
We address the issue of dynamic modeling and control of the Bluefin Odyssey III class vehicle "Caribou," operated by the MIT Sea Grant AUV Laboratory. Focus is on demonstrating a simple forward design procedure for the flight control system, which can be carried out quickly and routinely to maximize vehicle effectiveness. In many situations, the control loops are tuned heuristically in the field; frequent retuning is necessitated by the inevitable changes in vehicle components, layout, and geometry. Our paradigm here is that 1) a prototype controller is developed, based on an initial model, 2) this controller is then used to perform a very compact set of runs designed to identify the vehicle dynamic response, and 3) a revised, precision controller based on this improved model is implemented for the ultimate mission.

We first developed a hydrodynamic model of the vehicle from theory and benchtop laboratory tests; no data from prior field tests with this vehicle was used. Body added mass approximations were included as well as lift and hydrostatic forces and moments. Inertial properties were approximated by assuming the vehicle density was that of water. Caribou's tailcone assembly consists of a double-gimbaled thrust-vectoring duct, with significant positioning dynamics and a non-traditional hydrodynamics. We carefully tested this tailcone's response behavior through laboratory tests, and created a low-order model. Using the tailcone model and the vehicle's initial hydrodynamic model, we developed a conservative controller design from basic principles. The control system consisted of a heading controller, pitch controller, and depth controller; the pitch control loop was nested inside the depth control loop. This control system was successfully tested in the field: the vehicle was controllable within several degrees of heading and approximately one-half meter of depth, on the first-pass design.

System identification tests were then completed with the preliminary controller to gain a better understanding of the complete hydrodynamics of the vehicle, and in order to develop a precision controller based on the improved model. The resulting data provided a full-system linear model of the vehicle, and led to a successful controller redesign, with significantly improved performance.

Introduction
Developments made in Autonomous Underwater Vehicle (AUV) related technologies have enabled AUVs to move out of the research laboratory and into the commercial environment. AUVs are also used by the military, and a large portion of the AUVs in use today are still used in a scientific setting. Improvement in the performance of AUVs is needed to enhance the developments made in long-range oceanographic surveys, shallow-water mine reconnaissance and

countermeasures, and procedures in autonomous docking [1]. By improving the vehicle's control system, maneuvering becomes more precise and battery power is conserved. In order to develop a precise control system a finely tuned dynamic model of the vehicle is needed for testing and research purposes.

Previous work in dynamic modeling of AUVs includes simulation model verification done through field tests [2] as well as theoretical and empirical methods in addition to tow tank results [3]. Recent work done on AUV control has included gains obtained using partial model matching methods [4], as well as sliding mode control based on estimated coefficients [5], in addition to fuzzy sliding mode control systems [6]. Previous work in system identification of AUV systems has been done using neural network identifiers [7] and neurofuzzy identification techniques [8]. The work presented here focuses on development of dynamic models and control systems from first principles. The system identification tests and simulation process form a forward design process.

Odyssey III Class AUV Caribou

The platform for this research was a Bluefin Odyssey III class vehicle, Caribou, operated by the MIT Sea Grant AUV Laboratory. Since receiving this vehicle from Bluefin, the AUV Lab has used an in-house developed operating system, and made substantial modifications to the hull, including several large holes for sensors. We stress that the dynamic response of this vehicle, described in this paper, does not necessarily represent that of other Bluefin vehicles as delivered.

Figure 1: The Caribou AUV in short configuration

Caribou is highly maneuverable and has a variable configuration in length and payload. It can operate at a range of speeds, and it has a novel propulsor and control surface that consists of a double-gimbaled ring finned duct thruster, which allows for vectored thrusting. The duct thruster's angle is limited at ±15degrees in both the yaw and pitch plane, known typically as the rudder and elevator angles, respectively. The propeller is confined to the duct for protection, as well as enhanced flow capabilities. The duct also acts as a control surface. Thus, the Odyssey III class AUV does not need fins to control the vehicle motion because the duct and vector thrusting capability is sufficient to impose directional control. Figure 2 shows the duct thruster arrangement.

Figure 2: Caribou's ring fin duct thruster

The hull shape of the Odyssey III base vehicle is based on a Series 58, Model 4154 Gertler polynomial [9] with a length of 84in (2.13m) and a maximum diameter of 21in (0.53m). For this work, the body referenced coordinate frame is located along the symmetric axis of rotation at the midpoint of the AUV. In this body coordinate system the x-axis is along the symmetric line proceeding towards the nose of the vehicle. The y-axis extends towards the port side of the AUV, while the z-axis is directed upwards. Body referenced velocity in the x direction, surge, is denoted by u. Velocity in the body frame y and z directions is v, sway, and w, heave, respectively. Rotational velocity about the x-axis, roll velocity, is denoted as p. Rotational velocity about the y-axis and z-axis is q, pitch rate, and r, yaw rate, respectively. External body forces in the x, y and z direction are denoted as X, Y and Z respectively, while external body moments in the x, y and z direction are K, M and N respectively. The vehicle's angular orientation is described in the inertial frame of reference with Euler angles, ψ, θ, and φ.

Nonlinear Model

The external forces and moments resulting from the vehicle hydrostatics, hydrodynamic lift and drag, added mass, and the control input of the vehicle's ducted thruster are all defined in terms of specific coefficients for this model. Nonlinear equations were used to determine the vehicle's coefficients, and rigid-body dynamics. While the vehicle is inherently nonlinear, the nonlinear simulations provide more realistic simulations, but for control purposes, a linear model provides a sufficient platform, while maintaining less complexity.

In order to simplify the challenge of completely modeling an autonomous underwater vehicle, the

following assumptions about the vehicle and the environment were made for simulation purposes:

- The vehicle is a rigid body of constant mass
- The vehicle is deeply submerged in a homogenous, unbounded fluid
- The vehicle does not experience memory effects
- The vehicle does not experience underwater turbulence

Overall Vehicle Modeling

The vector transformation from an inertial frame of reference to the body frame is developed by using Euler angles (ψ,θ,ϕ), which describe the roll, pitch and yaw position of the vehicle in inertial space, as described by Crandall [10]. The general motion of the vehicle in six degrees of freedom is described by the following twelve states:

$$\vec{x} = \begin{bmatrix} x & y & z \end{bmatrix}^T \quad \vec{E} = \begin{bmatrix} \psi & \theta & \phi \end{bmatrix}^T$$

$$\vec{v} = \begin{bmatrix} u & v & w \end{bmatrix}^T \quad \vec{\omega} = \begin{bmatrix} p & q & r \end{bmatrix}^T$$

The locations of the vehicle centers of mass and volume (buoyancy) are defined in terms of the body-fixed coordinate system. The vessel inertial dynamics were derived from the physics of the system and are written as follows in the body-referenced frame. X, Y and Z are the external body forces applied in the body-referenced directions of x, y and z respectively.

$$X = m\left[\dot{u} + qw - rv + \dot{q}z_{CM} - \dot{r}y_{CM} + (qy_{CM} + rz_{CM})p - (q^2 + r^2)x_{CM}\right]$$
$$Y = m\left[\dot{v} + ru - pw + \dot{r}x_{CM} - \dot{p}z_{CM} + (rz_{CM} + px_{CM})q - (r^2 + p^2)y_{CM}\right]$$
$$Z = m\left[\dot{w} + pv - qu + \dot{p}y_{CM} - \dot{q}x_{CM} + (px_{CM} + qy_{CM})r - (p^2 + q^2)z_{CM}\right]$$

The angular dynamics were derived in a similar way. The body-referenced angular equations of motion also include translation and rotational accelerations as well as velocities.

$$K = I_{xx}\dot{p} + I_{xy}\dot{q} + I_{xz}\dot{r} + (I_{zz} - I_{yy})rq + I_{yz}(q^2 - r^2) + I_{xz}pq - I_{xy}pr + m[y_{CM}(\dot{w} + pv - qu) - z_{CM}(\dot{v} + ru - pw)]$$
$$M = I_{yx}\dot{p} + I_{yy}\dot{q} + I_{yz}\dot{r} + (I_{xx} - I_{zz})pr + I_{xz}(r^2 - p^2) + I_{xy}qr - I_{yz}qp + m[z_{CM}(\dot{u} + qw - rv) - x_{CM}(\dot{w} + pv - qu)]$$
$$N = I_{zx}\dot{p} + I_{zy}\dot{q} + I_{zz}\dot{r} + (I_{yy} - I_{xx})pq + I_{xy}(p^2 - q^2) + I_{yz}pr - I_{xz}qr + m[x_{CM}(\dot{v} + ru - pw) - y_{CM}(\dot{u} + qw - rv)]$$

Given the body-referenced coordinate system, and assuming a symmetric homogeneous body, the angular inertial properties can be approximated by a diagonal inertia tensor, assuming that the cross terms are nearly zero. The moments of inertia about the body frame origin were computed, treating the vehicle as a homogeneous body with the density of water. Caribou is generally ballasted to be approximately +5lbs buoyant, with the center of mass, z_{CM}, located below the center of volume z_{CV}. Due to the separation of the center of mass and the center of volume the hydrostatic righting moment is stabilizing in pitch and roll.

The thrust from the propeller can be directed at various orientations depending on elevator angle, $\delta_{E,}$ and rudder angle, $\delta_{R,}$ because the vehicle has a vectored duct thruster. Therefore, depending on the orientation of the duct frame the applied force in the body-referenced frame is:

$$\vec{F}_{B,thrust} = T_P \begin{bmatrix} \cos\delta_E \cos\delta_R \\ \sin\delta_R \\ -\cos\delta_R \sin\delta_E \end{bmatrix}$$

Since this force may not be coincident with the body axis, a moment is induced in the pitch and yaw directions due to the thrust. The vector, $\vec{r}_B^T$, is the vector from the origin of the body frame to the thrust referenced frame origin, and $x_P < 0$.

$$\vec{r}_B^T = \begin{bmatrix} x_P \\ 0 \\ 0 \end{bmatrix} \qquad \vec{M}_{B,thrust} = \left(\vec{r}_B^T\right) \times \vec{F}_{B,thrust}$$

The propeller thrust can be described as follows, where U_p is the speed of the water seen at the propeller, n_p is the propeller speed, D is the propeller diameter, and ρ is the water density. The thrust coefficient, K_T is approximated as a linear function of the advance ratio [16].

$$T_p = K_T \rho {n_p}^2 D^4$$

Hydrodynamics

The dominant non-linear axial drag coefficient is:

$$X_{u|u|} = -\frac{1}{2}\rho A_f C_D$$

where ρ is the density of the surrounding fluid, A_f is the vehicle frontal area, and A_p is the rectangular planform area (ld). The axial drag coefficient of the vehicle was estimated from the Hydat manual [11] as follows where the leading coefficient comes from Schoenherr's line [12].

$$C_D = 0.0040\frac{\pi A_p}{A_f}\left[1 + 60\left(\frac{d}{l}\right)^3 + 0.0025\frac{l}{d}\right] = 0.023$$

The method used for estimating the hull crossflow drag is analogous to strip theory, the method used to

calculate the hull added mass. The total hull drag is approximated as the sum of the drag on the two-dimensional cylindrical vehicle cross-sections. We will assume that without any control planes on the vehicle hull, the rolling drag is negligible. To estimate axial added mass, we approximate the vehicle hull shape by an ellipsoid for which the major axis is half the vehicle streamlined body length, and the minor axis half the vehicle diameter. The axial added mass is then computed based on Blevins analytical formula for an ellipsoid [14]. Vehicle added mass was calculating using strip theory on both cylindrical and cruciform hull cross sections. From Newman [15], the added mass per unit length of a single cylindrical slice is given as:

$$m_a(x) = \pi\rho R^2(x)$$

where ρ is the density if the surrounding fluid, and R(x) the hull radius as a function of axial position. Integrating over the length of the vehicle, we arrive at the coefficients for the cross flow added mass. We will assume that in absence of any fins, the rolling added mass term is negligible. The body force from lift is as follows:

$$L_{Body} = -\frac{1}{2}\rho A_p C_L u^2$$

where A_p is the rectangular planform area (ld). The following are in radian form [17]:

$$C_{L,pitch} = 0.131\cdot\delta_w \qquad C_{L,yaw} = 0.131\cdot\delta_v$$

The combined Munk Moment and lift moment is [17]:

$$M_{Body} = -\frac{1}{2}\rho A_p l C_M u^2$$

By interpolating between the values in Hoerner for several ratio of d/l, the following relationships were established for the short vehicle configuration.

$$C_{M,pitch} = 0.123\cdot\delta_v \qquad C_{M,yaw} = 0.123\cdot\delta_w$$

Tailcone

From the Principles of Naval Architecture the lift and drag of the duct, neglecting transient flow effects, are given by [12]:

$$L = \frac{1}{2}\rho A_{eff} U^2 C_L(\alpha) \qquad D = \frac{1}{2}\rho A_{eff} U^2 C_D(\alpha)$$

where,

$$C_L(\alpha) = \left(\frac{\partial C_L}{\partial\alpha}\right)\alpha + C_{Dc}\alpha|\alpha| \qquad C_D(\alpha) = C_{do} + \frac{C_L^{\,2}}{\pi ARe}$$

The minimum section drag coefficient, C_{do}, is 0.010 while the standard Oswald efficiency factor, e, is 0.90. The cross flow fin drag coefficient, C_{Dc}, is 0.81, while the aspect ratio and duct area are listed as:

$$AR = \frac{diameter}{chord} = 3.458$$

$$A_{eff} = diam.\times chord = 0.0498$$

McEwen and Streitlien [19] estimated dCl/dα for this ring wing shaped duct control surface on results from Milewski [20], which referred to previous work done [21], and [22]. They found from Milewski's thesis [20] that dCl/dα = 3.4855 for AR=1.25, and that from the DSRV report [20] that dCl/dα = 5.1566 for AR = 4.3716. Between these two points they interpolated with a function of the form seen in van Dykes equation, and fit the ring wing results by allowing multiplicative parameters, r and s, in the definition of lift coefficient and aspect ratio as follows:

$$\left(\frac{\partial C_L}{\partial\alpha}\right)_{\alpha=0} = \frac{2\pi r}{1+\frac{2}{sAR}+\frac{16}{\pi(sAR)^2}\log(1+\pi e^{-9/8}sAR)} = 5.1$$

where s and r are: $s = 4.305, \quad 2\pi r = 5.927$

This development leads to a lifting force, developed using a linearized equation for the lift force.

$$L = \frac{1}{2}\rho A_{eff} U^2 C_L(\alpha) = 131 U^2\alpha$$

The velocity of the ring fin duct in the body frame is a combination of the body translation velocity and rotational velocity:

$$\vec{v}^{\,Ro} = \vec{v}^{\,Bo} + \vec{\omega}^{\,B}\times\vec{r}^{\,BoRo} = \begin{Bmatrix} u \\ v \\ w \end{Bmatrix} + \begin{Bmatrix} p \\ q \\ r \end{Bmatrix} \times \begin{Bmatrix} x_R \\ y_R \\ z_R \end{Bmatrix}$$

The transformation matrix relating the ring frame of reference to the body frame is:

$$T_{R/B} = \begin{bmatrix} \cos\delta_R\cos\delta_E & \sin\delta_R & -\cos\delta_R\sin\delta_E \\ -\sin\delta_R\cos\delta_E & \cos\delta_R & \sin\delta_R\sin\delta_E \\ \sin\delta_E & 0 & \cos\delta_E \end{bmatrix}$$

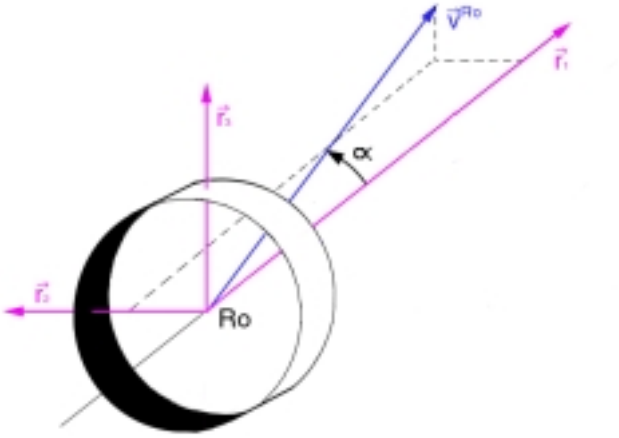

Figure 3: Duct coordinate frame

Using this transformation matrix, McEwen and Streitlien [19] computed the duct velocity in the ring frame and the angle of attack (Figure 3).

$$\vec{v}_R^{\,Ro} = T_{R/B}\vec{v}^{\,Ro} \qquad \alpha = \arcsin\frac{\left|\vec{v}_R^{\,Ro} \times \vec{r}_1\right|}{\left|\vec{v}_R^{\,Ro}\right|}$$

To form the transformation matrix that relates the ring frame to the forcing frame, the following vectors were established [19]:

$$\vec{t}_1 = \vec{v}_R^{\,Ro} \qquad \vec{t}_2 = \vec{v}_R^{\,Ro} \times \begin{Bmatrix} 1 \\ 0 \\ 0 \end{Bmatrix}$$

$$\vec{t}_3 = \vec{t}_1 \times \vec{t}_2 \qquad \hat{t}_i = \frac{\vec{t}_i}{\left|\vec{t}_i\right|}$$

Combining these vectors yields the transformation matrix for relating the ring frame to the forcing frame [19].

$$T_{R/LD} = \begin{bmatrix} \hat{t}_1 & \hat{t}_2 & \hat{t}_3 \end{bmatrix} \qquad \vec{F}_{LD} = \begin{bmatrix} -D \\ 0 \\ -L \end{bmatrix}$$

Combining the two transformation matrices and the forcing vector, the body referenced force from the duct control surfaces is calculated:

$$\vec{F}_{B,tailcone} = \vec{T}_{B/R}\vec{T}_{R/LD}\vec{F}_{LD}$$

This force is created at the duct location, thus inducing a moment about the body frame origin. This corresponding moment force is:

$$\vec{M}_{B,tailcone} = \vec{r}^{\,BoRo} \times \vec{F}_{B,tailcone}$$

Tailcone dynamics modeling

The actuation system of the Odyssey III AUV provided additional challenges in modeling and control of the system. Bench tests of the tailcone were also completed in order to develop a low-order model that encompassed the actuator dynamics as well as any computational delays in the system.

Caribou's actuation system is rate limited and deflection angle limited. In the field, Caribou's deflection angle limit is usually set to ±15 degrees for both the rudder and elevator angle. The rate limit was set at 15 degree/sec, which is dependent upon the actuator capabilities. In order to fully develop a model of the vehicle, as well as understand control strategies more fully, this actuation system needed to be modeled. To develop an understanding of the transfer function for the actuator, the system response was studied over a range of frequencies and amplitudes.

The heading/rudder tests were completed independently of the pitch/elevator tests. Figure 4 shows these results for the elevator tests. The cutoff frequency ranged from 1.5 to 4 rad/sec (0.24 Hz to 0.64 Hz) for the various heading/rudder tests. The stepper motors that control the rudder and elevator are rate limited actuators. Therefore, at larger peak to peak amplitudes, the cutoff frequency is less than for smaller peak to peak amplitudes commands. Caribou's tailcone is limited to travel 15degrees/sec. Therefore, for peak to peak amplitudes of 30 degrees, the highest frequency that can be passed without attenuation is 0.25 Hz (1.57rad/sec) because the time required, by the rate limited motors, to complete one cycle is 4 seconds. However, for a peak to peak amplitude of 10 degrees, the time required to complete one cycle is 1.33 seconds, which corresponds to a possible cutoff frequency of 0.75 Hz (4.71rad/sec).

In order to model the system about a controlled heading, the rudder and elevator actuation models needed to encompass how the response at lower amplitudes. Thus, the 2nd order model was modified to approximate the 10 degree peak-to-peak test data. Additionally, the phase plot in Figure 4 shows that there is much more phase lag at higher frequencies, than shown by a 2nd order model alone. Thus, in order to maintain this second order response with respect to magnitude, but add additional phase lag, a time delay was added to the system as described by Ogato [23].

The time constant *T* was set to 0.3, which resulted in an observed time delay of 0.3 seconds.

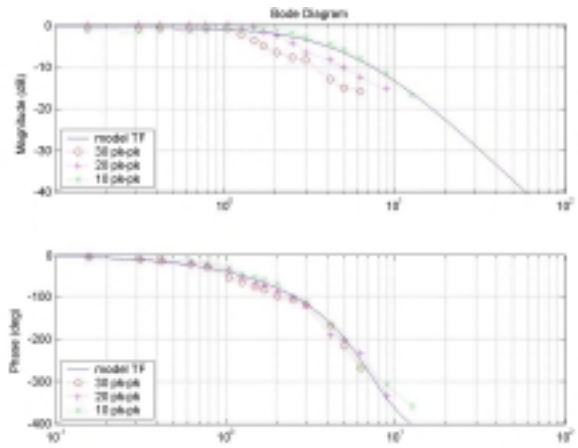

Figure 4: Elevator Modeling

$$G_{elevator\ actuator}(s) = \left[\frac{1}{\frac{3s^2}{100}+\frac{4s}{10}+1}\right]\left[\frac{\frac{9}{2}-\frac{Ts}{9}+\frac{(Ts)^2}{20}}{\frac{9}{2}+\frac{Ts}{9}+\frac{(Ts)^2}{20}}\right]$$

Linearized Model

The nonlinear equations of motion can be linearized and represented in matrix form. This system can be represented as a transfer function in the s-domain as follows:

$$\frac{\varphi}{\delta_R} = \frac{s\left[\frac{N_{\delta_R}}{(I_{zz}-N_{\dot r})}\right]+\left[\frac{-Y_v N_{\delta_R}+N_v Y_{\delta_R}}{(m-Y_{\dot v})(I_{zz}-N_{\dot r})}\right]}{s^3+s^2\left[\frac{-Y_v}{(m-Y_{\dot v})}+\frac{(mx_{CM}U-N_r)}{(I_{zz}-N_{\dot r})}\right]+s\left[\frac{-Y_v(mx_{CM}U-N_r)+(mU-Y_r)N_v}{(m-Y_{\dot v})(I_{zz}-N_{\dot r})}\right]}$$

The yaw acceleration as a function of deflection angle is found by differentiating this transfer function twice.

$$at\ \ s=\infty,\quad \frac{\dot r}{\delta_R}=\frac{N_{\delta_R}}{(I_{zz}-N_{\dot r})}$$

The instantaneous yaw acceleration as a function of rudder deflection angle is simply the moment forcing term, N_{dr}, divided by the mass term, (I_{zz}-N_{rdot}). Similar results are found in the pitch plane.

$$at\ \ s=\infty,\quad \frac{\dot q}{\delta_E}=\left[\frac{M_{\delta_E}}{(I_{yy}-M_{\dot q})}\right]$$

The instantaneous pitch acceleration as a function of elevator deflection angle is simply the moment forcing term, M_{de}, divided by the mass term, (I_{yy}-M_{qdot}).

Initial Controller Design

The controller development described in this work is based heavily on experimentally obtained data that was used to drive system identification. Based on an initial linear model of the AUV, a conservative initial controller was developed using Root Locus methods. Table 3 shows these initial gains. The goal of the control system design was to control the AUV within 10cm of the desired depth, as well as within 2 degrees of the desired heading.

Generally, an AUV such as Caribou will be tuned heuristically in the field, because in most cases the vehicle can be roughly tuned to control depth and heading after a short amount of time in the field. However, this rough control generally is refined by adjustments made to the controller during much further testing in the field. In addition, when the payload changes, the controller needs retuning. While this heuristic approach has worked satisfactory in the past, a more streamlined approach has many advantages over the numerous lost days of trial and error work in the field.

System Identification Process

The goal of this work was to develop an initial controller based on textbook models of the AUV. Using this controller, we could control the AUV to a desired depth and heading, accurately enough, so that we could turn the control system off and perform designed open-loop maneuvers. These open-loop system identification tests were performed in the field to help fit the model response to the responses seen in the field, by adjusting model coefficients and parameters. Using this improved model, an improved controller could then be developed. Figure 5, shows the process used to develop an accurate model and control system for the AUV.

The open-loop system identification maneuvers consisted of simple step responses of various angles for both rudder and elevator during separate missions. The thrust was kept constant during these step response tests, and the control system in the opposite plane was left on. Therefore, during a rudder step response mission, Caribou dove to a prescribed depth, maintained a rough heading and depth and then the heading controller was turned off while the rudder angle was set to a specific angle between 0 and ±15 degrees. Likewise in an elevator step response mission, at the prescribed depth the depth and pitch controllers were turned off while the elevator was set to a specific angle between 0 and +15 degrees. Note that only positive elevator angles were used to avoid hitting the sea floor since the tests took place in shallow water.

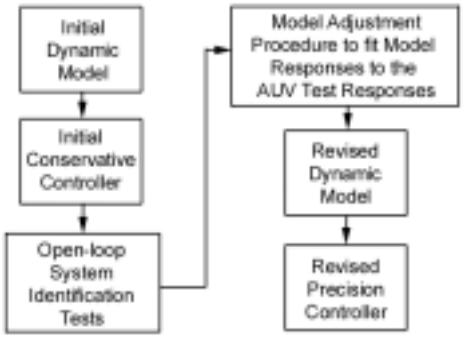

Figure 5: System ID Modeling & Control Process

Vehicle Simulation

After the open-loop response data was gathered in the field, the dynamic model parameters were adjusted to better fit the field data responses. Figure 6 shows the procedure used to adjust the model parameters.

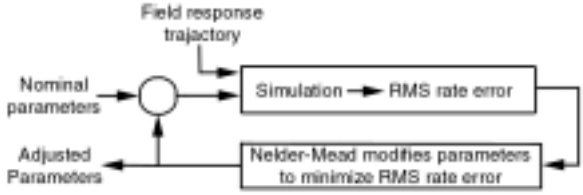

Figure 6: Model adjustment simulation process

The entire adjustment process was completed using Matlab scripts developed by the author. The simulation block consists of a 3-degrees of freedom (DOF) yaw plane and pitch plane, and a combined 6-DOF simulator as well. The process of parameter adjustment begins with picking which portions of data will be modeled. Thus, the recorded field data is screened for the step responses that provide consistent rates and no apparent unrepeatable system disturbances. The runs that were used had rudder angles smaller than 10 degrees, and all showed yaw rate transients with minimal pitch and depth response. Figure 7 shows a typical suitable yaw plane run for steps of 5° and 7°. The rudder had a -6° bias, therefore, Figure 7 shows actual rudder deflections of ±1°. Likewise, in choosing elevator step response runs for the simulation, runs with minimal heading change, and smooth pitch rate transients were chosen.

A decision must also be made on which parameters will be adjusted in the simulation and which parameters will be held constant. Given these initial input parameters and response runs, the simulation proceeds iteratively searching for a solution that minimizes the difference in the yaw rate of the field data with the yaw rate of the simulated response. In order to maximize the effectiveness of this process, only 3-DOF simulations are used. Hence, in the pitch plane simulation, the pitch rates are compared and the difference is minimized. The rates of all of the included runs are used simultaneously to establish an average error each time through the simulation. This allows various step responses with various deflection angles to all be encompassed together with one simulation.

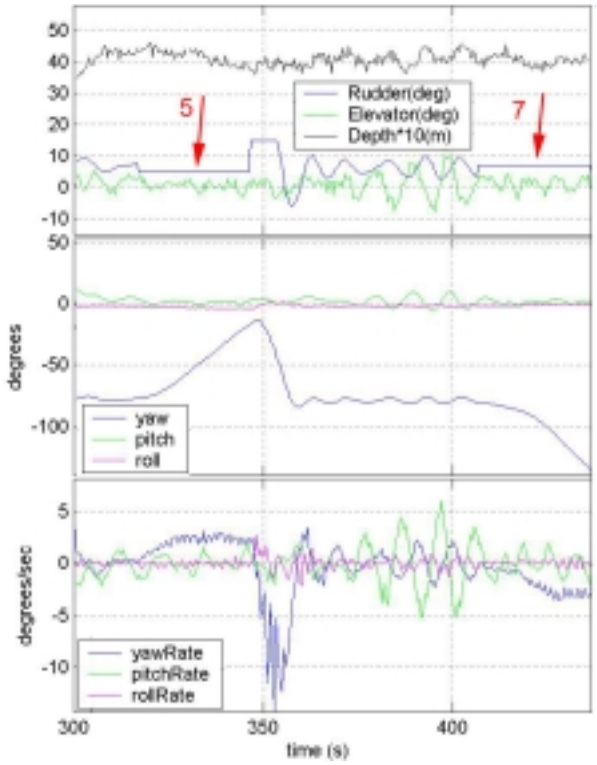

Figure 7: Rudder step response mission

In order to help determine which coefficients need to be adjusted, the transfer function of the AUV was analyzed for the yaw plane, and for the pitch plane.
Not all of the parameters that have a direct influence on the transfer function of the system need to be adjusted. The mass, m, weight, W, speed, U, and center of mass along the x-axis, x_{CM}, are quantities that are accurately known. In addition, the parameters I_{zz} and N_{rdot} are always coupled as $(I_{zz}\text{-}N_{rdot})$ and thus constitute only one parameter. Likewise, in the pitch plane $(I_{yy}\text{-}M_{qdot})$ is coupled. In addition, from step response data, the instantaneous acceleration rate per deflection angle is known.

$$\frac{\dot{r}}{\delta_R} = -0.51 \qquad \frac{\dot{q}}{\delta_E} = -0.46$$

Therefore, from the yaw acceleration rate transfer function, $(I_{zz}\text{-}N_{rdot})$ can be directly related to N_{dr}:

$$\left(I_{zz} - N_{\dot{r}}\right) = \frac{N_{\delta_R}}{\frac{\dot{r}}{\delta_R}} = \frac{N_{\delta_R}}{-0.51}$$

Likewise (I_{yy}-M_{qdot}) can be directly related to M_{de} as shown.

$$\left(I_{yy} - M_{\dot{q}}\right) = \frac{M_{\delta_E}}{\frac{\dot{q}}{\delta_E}} = \frac{M_{\delta_E}}{-0.46}$$

Therefore, the parameters to be adjusted in the yaw and pitch plane are reduced to:

$$Y_v \quad N_v \quad Y_r \quad N_r \quad Y_{\delta_R} \quad N_{\delta_R} \quad Y_{\dot{v}}$$
$$Z_w \quad M_w \quad Z_q \quad M_q \quad Z_{\delta_E} \quad M_{\delta_E} \quad Z_{\dot{w}} \quad z_{CM}\,.$$

	Initial Parameters	Adjusted Parameters	Percent Change
Thrust	58%		
U	1.3m/s		
Yv	-449	-445	-1%
Nv	-239	-159	-33%
Yr	266	331	24%
Nr	-525	-520	-1%
Ydr	251	264	5%
Ndr	-447	-513	15%
Yvdot	-632	-616	-3%
Izz	469	548	17%
Nrdot	-458	-458	0%
Zw	-449	-450	0.2%
Mw	239	157	-34%
Zq	-266	-343	29%
Mq	-525	-599	14%
Zde	-251	-270	8%
Mde	-447	-514	15%
Zwdot	-632	-652	3%
Iyy	469	659	41%
Mqdot	-458	-458	0%
zCM	-0.021	-0.015	-29%

Table 1: Original and adjusted

The original dynamic model was used to determine the initial controller. This initial model was adjusted based on the data from the system identification tests. The yaw plane model adjustments were completed first, and these improved coefficients were then used as the initial parameters for the pitch plane simulation, which allowed a closer model/data match. While the initially developed coefficients were the same for both the pitch and yaw plane models, the adjusted model, does not maintain this strict symmetry as is seen in Table 1. About half of the coefficients are similar between the two planes, within 5%-10%. The larger differences are likely do to some lack of sufficient data in the pitch plane, and perhaps may also be due, in part, to some error in the adjusted model. The one major difference is that between I_{zz} and I_{yy}, which may be due to the ballasting of the particular payload used during the system identification tests.

Figure 8 shows a step response for a rudder angle of +15°. The raw data from the field is shown, as well as the responses for the initial and improved model. Notice that the improved model is a better approximation to the actual response than the initial model. Therefore, heading controller designs based on this improved model would be thought to have better results when tried in the field.

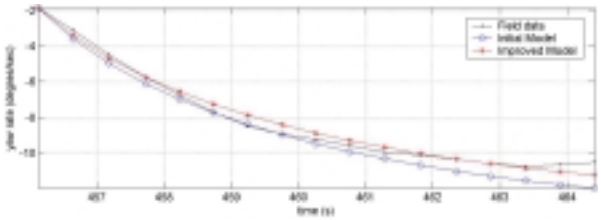

Figure 8: Yaw model improvements, +15° rudder

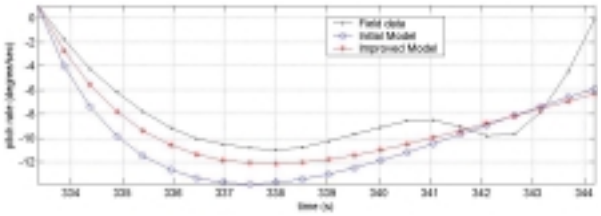

Figure 9: Pitch model improvements, +15° elevator

Figure 9, shows the step response for an elevator angle of +15°. The improved pitch model more closely models this field response. In these figures the adjusted models do not perfectly model the field data. One of main reasons this does not happen, is that the simulation adjustment process takes into account numerous runs with various deflection angles. The model is adjusted to approximate all of these runs simultaneously and therefore, more exact results are difficult to attain. Due to slight changes in the alternate plane as well as environmental effects, the actual rates for each step response are not textbook data sets. However, these figures show that measurable improvements in modeling are made by simply using step response tests. To develop a very precise model, several other system identification tests would need to

be used in the field to capture the various dynamic effects. However, for improvements in control design, this simple approach works well.

Table 2 lists the rate error for each model as compared to the field data rate. Notice that the improved model is more accurate than the initial model in modeling the AUV dynamics.

	Average Rate Error Squared	
Angle	**Initial Model**	**Improved Model**
15° rudder	0.37	0.11
15° elevator	7.96	3.71

Table 2: Model improvements

Controller Redesign

Using the improved model, an improved controller was developed and used for closed loop comparison tests. Table 3 lists the gains for the initial and improved controllers.

	Heading			
Controller	Kp	Kd	Ki	Ki limit
Initial	0.65	1.5	0.001	0.01
Improved	0.55	1.35	0.01	0.1
	Pitch to Elevator			
Controller	Kp	Kd	Ki	Ki limit
Initial	0.8	1.9	0	0
Improved	0.55	1.2	0	0
	Depth to Pitch			
Controller	Kp	Kd	Ki	Ki limit
Initial	0.13	0	0.001	0.004
Improved	0.12	0	0.004	0.05

Table 3: Controller gains used in the field

The heading controller controls on the error in heading angle and has output of desired rudder. This controller is aggressive and works to eliminate steady state error as well. The depth to pitch controller controls on the error in vehicle depth, and has output of desired pitch. This outer depth loop is only as quick as the AUV is capable of reaching desired depths and pitch angles. The depth loop is slower than most loops, and thus does not have a derivative gain. The pitch to elevator loop is nested inside the depth loop and it controls on the error in the vehicle's pitch. This loop has output of desired elevator. The pitch loop does not have an integrator gain, because the depth loop has one and the ultimate goal is to control about a depth and not a pitch, therefore, elimination of steady state error in depth is more important than elimination of steady state error in pitch. Table 4 shows the improvements made to the dominant closed loop pole positions in the control loops for the initial and the improved model. The improved model has greater damping in all three loops.

Model	Controller	Heading Poles
Initial	Initial	-1.0086 ± 1.8438i
Improved	Initial	-1.0730 ± 1.5458i
Improved	Improved	-1.2057 ± 1.4678i
		Pitch Poles
Initial	Initial	-0.8257 ± 1.8075i
Improved	Initial	-0.8941 ± 1.4726i
Improved	Improved	-1.1786 ± 0.9619i
		Depth Poles
Initial	Initial	-0.7766 ± 1.6955i
Improved	Initial	-0.8277 ± 1.3390i
Improved	Improved	-1.1520 ± 0.7876i

Table 4: Dominant closed loop poles

Closed Loop Controller Comparisons

The initially designed controller and the redesigned controller were used separately for the same missions to verify the improvements made through system identification tests, redeveloped models and redesigned controllers.

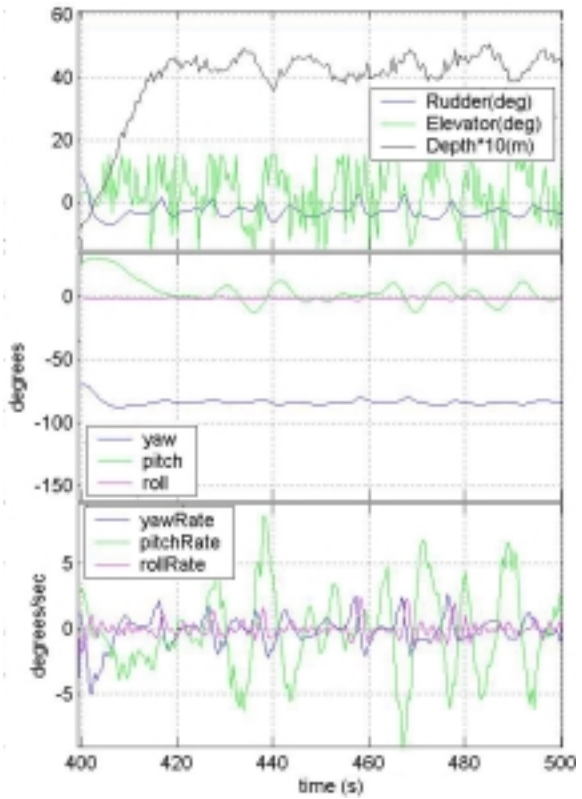

Figure 10: Straight run with initial controller

Straight Run

Figures 10 and 11 display two straight runs at a controlled heading and a controlled depth. The mission shown in Figure 10 was made using the initial controller, while Figure 11 was made using the improved controller in the field. As expected from

the gains used, the heading control is very similar for each run, while the pitch and depth control seem to be much better with the improved controller.

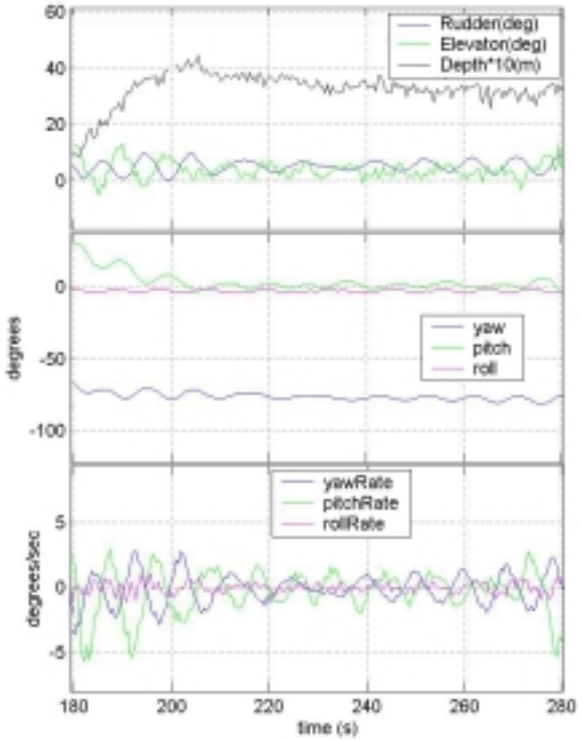

Figure 11: Straight run with improved controller

Table 5 shows the comparisons between the initial and improved controllers, for the error during steady state flight. The pitch and depth loops were improved substantially, while the heading loop was initially designed well, and thus improvement in heading control was minimal.

Controller	Initial	Improved
Heading Error	± 2.5°	± 2.0°
Pitch Error	± 10°	± 2.5°
Depth Error	± 50cm	± 10cm

Table 5: Closed-loop improvements

Depth Change Run

The depth change mission with constant heading is shown in Figure 12 and 13. Again, the system using the improved controller responds much better to the commands, than the system that uses the initial controller.

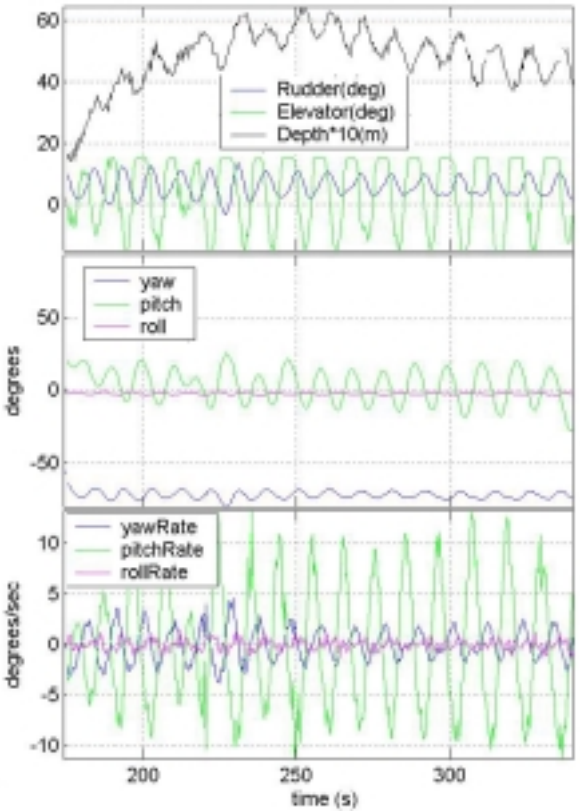

Figure 12: Depth change run with initial controller

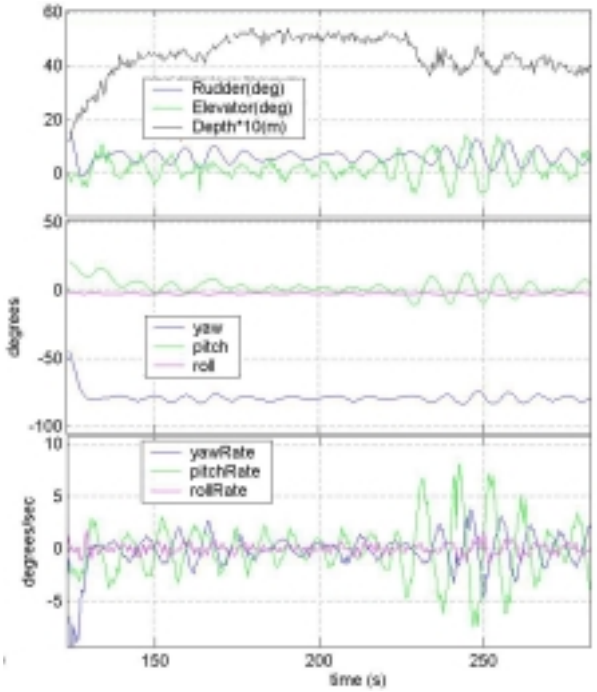

Figure 13: Depth change run with improved controller

Large Depth and Heading Change

A very aggressive mission was a coupled depth and heading change maneuver. This test was completed

only with the improved controller. The vehicle was commanded to 4m depth at -80° heading for 30 seconds and then to 7m depth at -40° heading for the next 60 seconds. For the last 60 seconds the AUV was commanded to 1m depth at -100° heading. As you can see from Figure 14, Caribou performed these maneuvers remarkably well while using the improved controller.

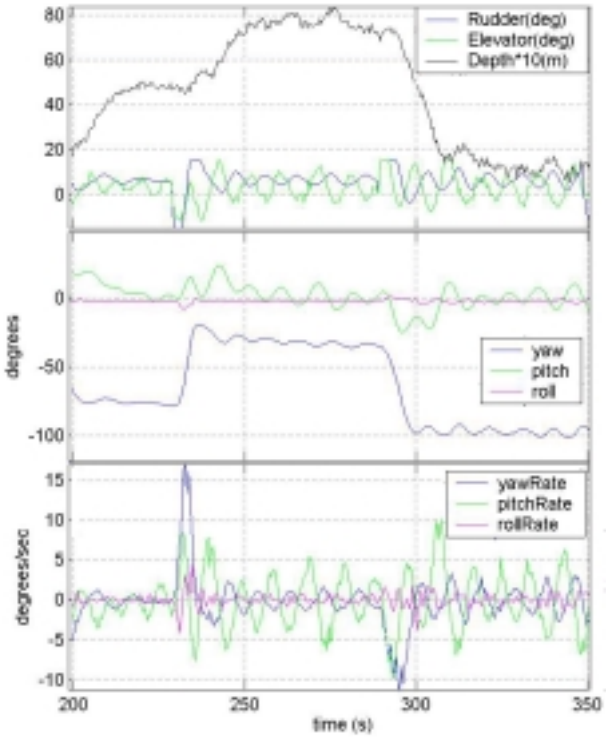

Figure 14: Improved control heading & depth change

Shallow 1m Depth Run

The final closed-loop maneuver was a shallow, 1m depth mission. The thought was that this may be very difficult considering that surface effects at shallow depths may cause the vehicle to surface. Figure 15 displays a 1m depth run in which the improved controller was utilized. After an initial overshoot, Caribou held the desired depth of one meter very well. These results suggest that maneuvering under the Arctic ice may be possible at very shallow depths, although that case represents a hard boundary as opposed to a free surface.

Future Work

The simple system identification step response tests may not have excited all of the interesting dynamics of the AUV, and thus, several other different tests could be utilized in the future in order to develop a better list of dynamic coefficients. These tests may include runs in which sinusoidal rudder or elevator commands are used in open-loop tests. Other tests that would be useful are speed and acceleration tests, as well as working through all of the tests at various levels of thrust.

Several improvements need to be made to Caribou. First, an improved tailcone system should be implemented that does not operate using the stepper motor system currently being utilized, since the current setup can lead to large errors in actual position vs. commanded position. Ideally this new system would allow for duct position feedback that can be recorded as a mission variable. This improvement would allow for a much greater ease in model simulation, as the actual duct position would be known and not inferred from the commanded position.

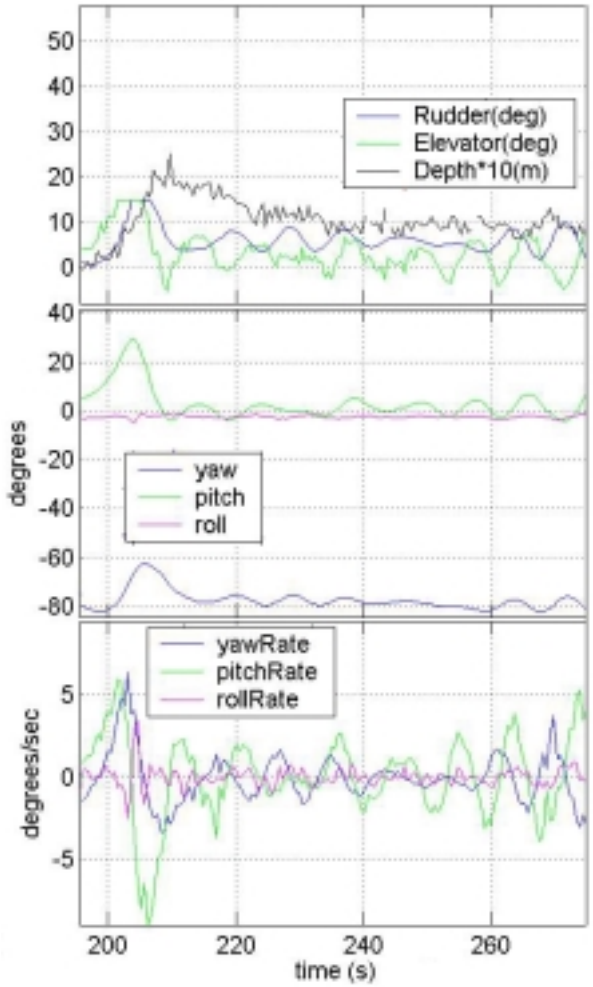

Figure 15: Improved control shallow run at 1m depth

Summary and Conclusions

A dynamic model of the Odyssey III Class Autonomous Underwater Vehicle, Caribou, was initially developed in order to develop a control system for this AUV. The dynamic model included

hydrodynamic and hydrostatic effects, as well as inertial and added mass characteristics. The tailcone system, which consists of an adjustable vector duct thruster was tested and modeled in a laboratory setting. An initial control system was designed for the heading, pitch and depth control loops, based on a linearized model from the combined nonlinear model.

A series of open-loop step response tests were completed in the yaw and pitch planes independently. Using these results, and the simulation model, the linearized coefficients from the initial model were adjusted so that the simulation response closely matched the response seen in the field for the same step input in rudder or elevator commands. Using this improved model, the control gains were redesigned.

Results from closed-loop tests showed that the redesigned controller was superior to the initially designed controller. These results show that a systematic approach to controller design, that is based on first principles does not only work, but produces results that are hard to attain through heuristic tuning alone. This work shows that by performing a few hours worth of tests, and then running the simulation process with the recorded data, the proper control gains for an AUV can be discerned in only a very short amount of time, while conventional methods can lead to days, if not weeks, of tuning in the field. This work shows that time and money can be saved by using a systematic approach to control.

References

[1] H. Singh, M. Bowen, F. Hover, P. LeBas, and D. Yoerger, "Intelligent Docking for an Autonomous Ocean Sampling Network." Proceedings of the 1997 Oceans Conference, Halifax, NS, Canada. 1997.

[2] T. Prestero, "Development of a Six-Degree of Freedom Simulation Model for the REMUS Autonomous Underwater Vehicle." Oceans 2001 MTS/IEEE, Honolulu, HI. 2001.

[3] M. Seto and G. Watt, "Dynamics and Control Simulator for the Theseus AUV." Proceedings of the International Offshore and Polar Engineering Conference, Seattle, WA. 2000.

[4] S. Miyamoto, T. Aoki, T. Maeda, K. Hirokawa, T. Ichikawa, T. Saitou, H. Kobayashi, E. Kobayashi, and S. Iwasaki, "Maneuvering Control System Design for Autonomous Underwater Vehicle." Oceans 2001 MTS/IEEE, Honolulu, HI. 2001.

[5] J. Kim, K. Kim, H.S. Choi, W. Seong, and K.Y. Lee, "Depth and Heading Control for Autonomous Underwater Vehicle Using Estimated Hydrodynamic Coefficients." Oceans 2001 MTS/IEEE, Honolulu, HI. 2001.

[6] P. Le, and K.W. Holappa, "Simulation and Control of an Autonomous Underwater Vehicle Equipped with a Vectored Thruster." Oceans Conference Record (IEEE), Piscataway, NJ. 2000.

[7] H. Sayyaadi, and T. Ura, "Multi Input-Multi Output System Identification of AUV Systems by Neural Network." Proceedings of the OCEANS '99 MTS/IEEE, Seattle, WA. 1999.

[8] K.M. Bossley, M. Brown, and C.J. Harris, "Neurofuzzy Identification of an Autonomous Underwater Vehicle." International Journal of Systems Science, Southampton, UK. 1999.

[9] M. Gertler, "Resistance Experiments on a Systematic Series of Streamlined Bodies of Revolution – For Application to the Design of High Speed Submarines." Navy Department, David W. Taylor Model Basin, Report C-297. April 1950.

[10] S.H. Crandall, D.C. Karnopp, E.F. Kurtz, Jr., and D.C. Pridmore-Brown. "Dynamics of Mechanical and Electromechanical Systems." Robert E. Krieger Publishing Co. Malabar, FL. 1968.

[11] Hydat manuel, Draper Laboratory, Cambridge, MA. 1988.

[12] E.V. Lewis, "Principles of Naval Architecture, Vol. II." The Society of Naval Architects and Marine Engineers, Jersey City, NJ. 1988.

[13] S.F. Hoerner, "Fluid Dynamic Drag." Published by Author, Midland Park, NJ. 1958.

[14] R.D. Blevins, "Formulas for Natural Frequency and Mode Shape." Robert E. Krieger Publishing Co. Malabar, FL. 1984.

[15] J. N. Newman, "Marine Hydrodynamics." MIT Press, Cambridge, MA. 1980.

[16] M.S. Triantafyllou, and F.S. Hover, "Maneuvering and Control of Marine Vehicles." Course Notes 13.49, Ocean Engineering Department, Massachusetts Institute of Technology. 2001.

[17] S.F. Hoerner, "Fluid Dynamic Lift." Published by Author, Vancouver, WA. 1985.

[18] H. August, "Ring Wing for an Underwater Missile." Journal of Aircraft, v 33, n 4. 1996.

[19] R. McEwen, and K. Streitlien, "Modeling and Control of a Variable-Length AUV." Monterey Bay Aquarium Research Institute, Moss Landing, CA. July, 2001.

[20] W.M. Milewski, "Three-dimensional Viscous Flow Computations Using the Integral Boundary Layer Equations Simultaneously Coupled with a Low Order Panel Method." PhD

Thesis, Massachusetts Institute of Technology. June, 1997.

[21] W. B. Morgan and E. B. Caster, "Prediction of the Aerodynamic Characteristics of Annular Airfoils." Technical Report 1830, David Taylor Model Basin. 1965.

[22] C. Broxmeyer, et. al., "Deep Submergence Rescue Vehicle Simulation and Ship Control Analysis." Technical Report R-570-A, Instrumentation Laboratory, Massachusetts Institute of Technology, Cambridge, MA. February, 1967.

[23] K. Ogato, "Modern Control Engineering." Prentice-Hall Inc., Englewood Cliffs, NJ. 1970.

[24] M. Abkowitz, "Stability and Motion Control of Ocean Vehicles." MIT Press, Cambridge, MA. 1972.

[25] E.V. Lewis, "Principles of Naval Architecture, Vol. III." The Society of Naval Architects and Marine Engineers, Jersey City, NJ. 1989.